17th World Conference on Earthquake Engineering, 17WCEE
Sendai, Japan - September 13th to 18th 2020

SEISMIC COLLAPSE ANALYSIS OF CONFINED AND UNCONFINED URM BUILDING WITH DISCRETE FINITE ELEMENT MODELLING

Trissa Deb[(1)], Terry Y.P. Yuen[(2)], Yang Liu[(3)], Rudhra Halder[(4)]

[(1)] *Ph.D. Candidate, National Chiao Tung University, Taiwan, R.O.C., trishadeb23@gmail.com*
[(2)] *Assistant Professor, National Chiao Tung University, Taiwan, R.O.C., terryyyp@nctu.edu.tw*
[(3)] *Associate Professor, College of Civil Engineering, Huaqiao University, China, yliubp@hqu.edu.cn*
[(4)] *Ph.D. Candidate, National Chiao Tung University, Taiwan, R.O.C., rudhrahalder@gmail.com*

Abstract

Masonry is a nonhomogeneous, inelastic and anisotropic material comprising of two different units, i.e. masonry block and mortar joint, of two different properties. Masonry is weak in tension because it is an assemblage of brick and mortar distributed periodically and the bond between them is weak. Thus, masonry walls are designed and expected to resist compressive forces only. Confined masonry structures i.e. masonry with vertical tie-column are extensively constructed in various parts of the world. Tie-column does not generally represent the load-bearing part of a structure but prevents disintegration and improves the ductility of masonry structure under the influence of lateral load. Tie-columns are generally placed at corners, wall intersections, etc. and the amount of reinforcement generally depends on experience, utility, and configuration of the structure. A well-built confined masonry structure can survive major earthquakes without collapse and in most cases without significant damage. In this regard, the paper numerically investigates the seismic performance and collapse potential of confined and unconfined URM (unreinforced masonry) structure.

The modelling approach is based on the use of contact-interaction with discrete finite element modelling (DFEM) where the masonry is treated as a distinct deformable-body i.e. discrete element separated by a predetermined gap. No interfacial element exists between the masonry unit to characterize the mortar joint and the response of the mortar joint are modelled by means of interaction between the masonry units using a novel interfacial constitutive law “coupled damage plasticity traction-separation law with fracture energy-based softening rules” which has been successfully implemented in ABAQUS with user-subroutine VUINTERACTION.

Incremental dynamic analysis (IDA) with the rigorous and detailed DFEMs was performed to investigate the collapse probability of masonry structure at different earthquake intensity levels. Damage-plasticity traction-separation law along with DFEMs could capture the crack propagation, stiffness degradation, disintegration and progressive collapse of masonry structure efficiently. Masonry panels in the vicinity of openings demonstrate a ratcheting phenomenon due to the propagation of sliding cracks developed from the stress concentration regions about the corner of the opening. For confined masonry structure, the contribution of tie-column is significant after cracking of masonry wall due to maximum resistance. This is owing to the dowel mechanism of tie-column reinforcement which improves the performance of the masonry structure.

Keywords: masonry structure; discrete finite element; seismic vulnerability; incremental dynamic analysis; tie-column

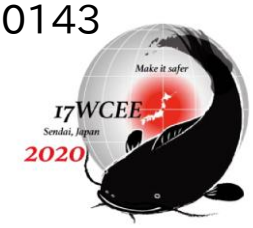

1. Introduction

Unreinforced masonry (URM) is one of the oldest and widespread structural types even though they are highly susceptible to damage from earthquakes. The failure of masonry structures has a huge impact on human civilization as it constitutes a major part of the habitat for ordinary people. Earthquakes are one of the deadliest natural disasters yet casualty does not occur directly due to ground motions but as a consequence of the collapse of structures. Recent earthquakes suggest that the majority of masonry structure fail due to fracture of mortar joints and crushing of masonry components. Lateral loads can produce both diagonal cracking failure and horizontal bed shear failure modes which are predominantly observed in masonry structures. Frictional resistance at the interface is mostly observed in older load bearing unreinforced masonry structure which acts in combination with shear [1]. Accurate and reliable investigation of force-deformation behavior of masonry structures subjected to different types of loading is the most crucial step towards a robust and safe design of masonry structures.

Masonry structures perform reasonably well under gravity load due to inherent compression carrying capacity but inadequate shear and tension carrying capacity render vulnerability to these structures during an earthquake. Brick masonry structures are extremely popular in housing construction comprising of brick and mortar distributed at regular intervals. These two materials are joined by a weak interface with low tensile strength and shear cohesion but capable to resist in-plane shear failure. Lateral load causes out-of-plane collapse which is the most common mode of failure in masonry structures accompanied by shear cracks in walls generally initiated at the corner of the wall opening. For larger span length, out-of-plane failure causes the wall to topple due to poor wall-roof connection which further leads to the disintegration of floors and roofs and total collapse of the structure in the worst scenario. Thus, wide research has been carried out in this domain to improve the performance of URM structures in order to increase the collapse time under earthquake loading thereby reducing the loss of lives from sudden disastrous collapse of the structure. In lieu of the above, confined masonry structures are expected to provide better performance under lateral load compared URM structures and reinforced concrete frames with infill [2]. In confined masonry structures, the masonry walls carry earthquake load and tie column enhance the stability, integrity, and ductility of the structure thereby improving seismic performance. Numerous experimental and analytical studies have been conducted previously to predict the seismic behavior of confined and unconfined masonry structures. Marques and Lourenco [3] experimentally studied the behavior of unreinforced masonry and confined masonry structure and compared it against the pushover response of the corresponding computational model. Tomazevic and Klemenc [4] experimentally verified the seismic performance of confined masonry wall and it was observed that tie-columns significantly improve the ductility of a masonry building. From the experimental results and observed behavior, a rational method was developed to model the seismic behavior of confined masonry wall. Alocer *et al.* [5] studied the dynamic response of confined masonry building particularly in Mexico through shake table tests.

Numerical modelling of masonry structures can be broadly classified into three categories: (a) macroscopic modelling with the strut-and-tie model, (b) homogenisation of the masonry units and mortar joints with uniform constitutive law and (c) microscopic modelling with distinct elements and constitutive laws for masonry units and mortar joints. In the first approach, the strut represents the compression element and the tie as tensile reinforcement in masonry structure [6]. The macroscopic modelling provides a quick estimation of global strength and stiffness of the structure but fails to capture a detailed three-dimensional response. The homogenisation of mesoscopic modelling balance the analysis accuracy and computation demand of strut-and-tie models and microscopic models [7]. The constitutive model of the homogenised masonry continuum generally depends on masonry configuration, bonding method (characterised by the representative volume element RVE), failure mechanisms and thus if these features are changed recalibration of model is essential [8]. The microscopic modelling is the most accurate among the three approaches but requires higher computational costs [9]. The model parameters are directly related to material properties i.e. masonry unit and mortar and independent of structural configuration thus can be applied for different structural configuration and loading conditions [10]. The emerging discrete element modelling (DEM) and

discrete finite element modelling (DFEM) can simulate the structural collapse due to the disintegration of components which is not possible in the conventional continuum model [11].

The paper presents an analytical study of seismic performance and collapse analysis of confined and unconfined unreinforced masonry structure with discrete finite element modelling. Fracture energy-based damage-plasticity traction-separation law with discrete finite element modelling developed by Yuen *et al*. [11] was utilized to model the interaction between the masonry units implemented in ABAQUS [12] using user-subroutine VUINTERACTION. Nonlinear response history analysis under bi-directional excitations are performed with five real ground motions at different intensity level. System Identification (SI) was utilized to determine natural frequency and subsequently time period at the first mode of vibration for the structures. System Identification (SI) is the procedure to construct a mathematical model of an unknown system based on a set of input-outputs and is practiced in different fields of engineering [13]. The seismic performance of the structure in terms of IDA curve, stress distribution and damage pattern and presented in the subsequent sections.

2. Prototype Masonry Structure

The prototype structure is a one-storey building with four masonry panels on four sides and different door and window configuration. The dimension of the masonry structure is 5000 x 3000 x 3000 mm (Fig. 1(a), 1(b)) rested upon a concrete foundation slab of 250 mm depth. The top concrete roof slab is 120 mm thick and reinforced with steel bars of 10 mm diameter spaced at a distance of 300 mm. For confined masonry structure, the masonry walls are bounded by RC columns on the four sides as shown in Fig. 1(b). The size of RC column is 250 x 250 mm reinforced with four steel bars of 10 mm diameter. The Young's moduli of concrete, masonry, and rebar are considered as 10 GPa, 5.46 GPa, and 215 GPa respectively. The modelled tension and compression behavior of masonry units are determined based on the recommendations by CEB-FIP model code [14] as shown in Fig.2.

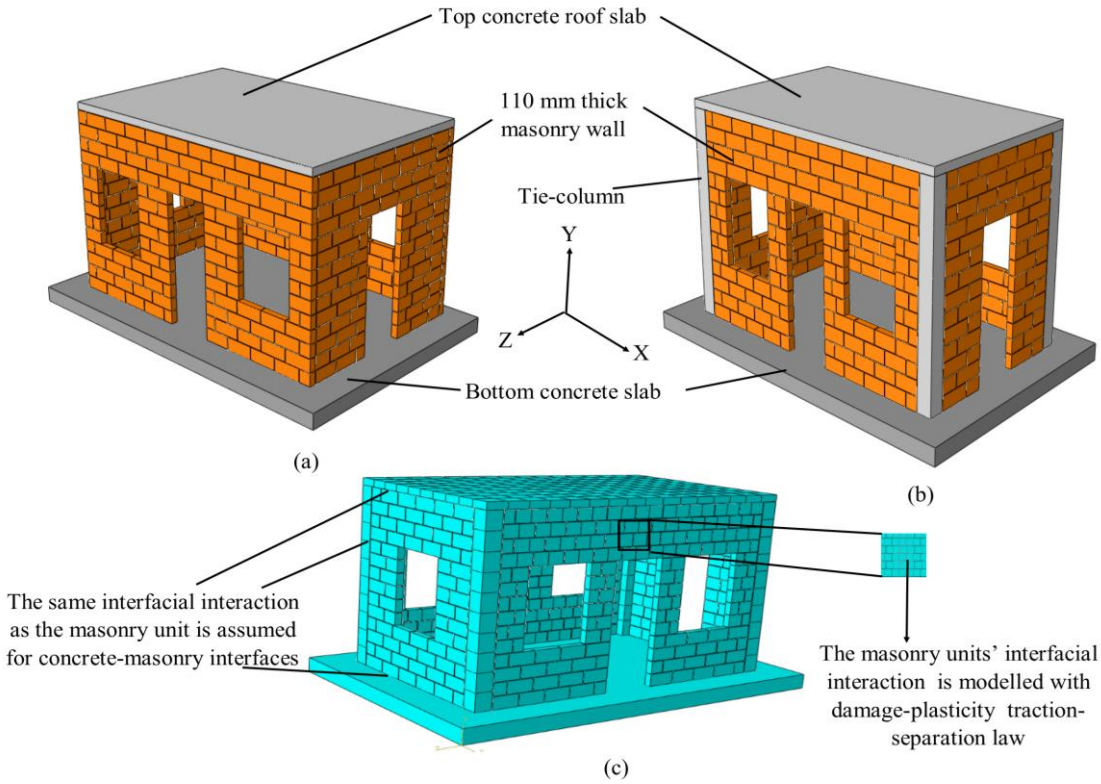

Fig. 1 – Geometry of prototype unreinforced masonry structure (a) unconfined (b) confined (c) meshing and interaction.

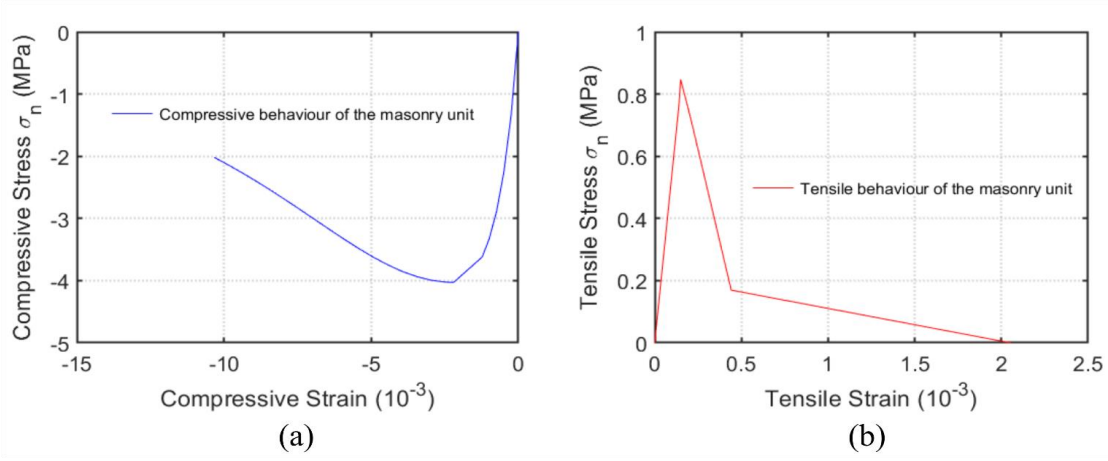

Fig. 2 – Stress-strain behavior of masonry units under (a) compression and (b) tension.

The masonry units and the concrete slab are meshed with three-dimensional 8-node linear brick elements as shown in Fig. 1(c). The brick units are separated by 10 mm to account for the thickness of the mortar joint. No reduced integration is considered for the element mesh as it would result in significant fluctuation in the contact stresses.

3. Discrete Finite Element Model

3.1 Discrete finite element modelling

The most detailed and rigorous modelling of masonry structure by finite element methods is to mesh the structure as of original geometry and enforce appropriate stress-strain laws for individual materials. This approach is known as micro-modelling which obviously requires higher computational time to simulate load-deformation behavior due to the larger number of elements [15]. Also, the size of the element has to be sufficiently small for mortar joint mesh to prevent elements with higher aspect ratios which may undergo excessive distortion on the onset of inelastic deformation that can affect simulation accuracy. The strength of the mortar joint is often weaker than the masonry unit in the masonry wall, so damage and cracks most likely propagate along the joints. Thus, the conventional micro-modelling approach is seldom utilized for practical design and analysis of large masonry structures.

When the masonry structure is subjected to in-plane horizontal loading or out-of-plane bending, cracks propagate along mortar joint or interfaces between the brick and mortar forming a “stepping down” crack pattern. In light of such predominant failure modes, the mortar joint can be homogenised and modelled by traction separation law between the bonded brick surface. In this approach, the physical space of the mortar joint is absorbed by the brick to form the “continuum element” of the masonry wall. The opposite faces of the adjacent expanded element are connected by zero thickness element or through contact interaction where the traction-separation law is enforced. In this zero-thickness modelling, unrealistic penetration of element/surface may occur under high compression. In DFEM [12], the masonry units are treated as individual deformable bodies i.e. discrete element separated by a finite gap. Unlike DEM, where the discrete elements are considered as rigid bodies, in DFEM, the elements are discritised as finite continuum element based on which deformation and constitutive relations can be defined. No interfacial element exists between the masonry unit to model the mortar joint and the mortar joints are modelled as the interaction between the masonry units using the interfacial contact law, i.e. the coupled damage-plasticity traction-separation law proposed by Yuen *et al.* [11] implemented in ABAQUS [12] using user-subroutine VUINTERACTION. Like DEM, DFEM is extensively applicable for addressing problems such as fracture, dislocation and shear

band problems simultaneously simulating the deformation of elements under internal stress [16]. For the present study, DFEM is applicable because cracks in the mortar joint lead to discontinuities and masonry units are deformable, thus it is not suitable to consider them as rigid elements.

As long as the separation of the two interacting surfaces is within the tracking thickness, the interaction calculated by the surface constative law will not vanish. Hence, it is possible to retain the original size of the brick units and define the initial gap to be the same as the mortar joint thickness. Yet, the tracking thickness should be sufficiently large to account for the cracking opening displacements. This approach, known as the simplified micro-modelling method, can greatly reduce the computation time by eliminating the elements originally needed for meshing the thin mortar joints in the micro-modelling method. The general three-dimensional traction-separation law reads as follows:

$$\begin{bmatrix} \sigma_n \\ \tau_1 \\ \tau_2 \end{bmatrix} = \begin{bmatrix} k_n & 0 & 0 \\ 0 & k_{s1} & 0 \\ 0 & 0 & k_{s2} \end{bmatrix} \begin{bmatrix} \delta_n^e \\ \delta_{s1}^e \\ \delta_{s2}^e \end{bmatrix} \text{ or } \sigma = k_e.\delta^e \tag{1}$$

where, $\delta^e=\delta-\delta^p$ is the elastic displacement of the total displacement vector δ in which δ^p is the plastic displacement; σ is the traction vector of the normal traction σ_n (corresponding to the normal displacement δ_n^e)and the shear tractions in two perpendicular horizontal directions τ_1 and τ_2 (corresponding to the shear displacements s_1^e and s_2^e respectively); k_e is the effective elastic stiffness matrix. It can be observed that the Poisson's effect is ignored in Eq. (1) which may be the major limitation of the simplified micro-modelling method with traction-separation law. The rate form of Eq. (1) is

$$\dot{\sigma}=k_e \cdot \dot{\delta}^e+\dot{k}_e \cdot \delta^e \tag{2}$$

The first term is the classic elastic stress-deformation incremental relationship, while the second term is non-zero only if the elastic stiffness constants change during the load-deformation process, i.e. $\dot{k}_e = \sum\left(\partial k_e / \partial \xi_i\right) \cdot \dot{\xi}_i + \partial k_e / \partial t$,where, $\dot{\xi}_i$ is the rate of internal variables affecting the stiffness such as damage variables or accumulated plastic deformation. The second term $\partial k_e / \partial t$ can be used to account for the stiffness change due to time-dependent processes such as cement hydration and other aging effects.

3.2 Incremental inelastic traction-separation relationship

To implement the coupled damage-plasticity traction-separation model in general FE codes, an incremental form of the constitutive relationship shall be established. The incremental form of Eq. (2) can be rewritten as

$$\Delta\sigma=k_e \cdot \left(\Delta\delta-\Delta\delta^p\right)+\delta^e \cdot \left(\frac{\Delta k_e}{\delta d^p} \cdot \Delta\delta^p\right) \tag{3}$$

The plastic displacement increment and the crack displacement increment are

$$\Delta\delta^p = \Delta\lambda \frac{\delta G}{\delta\sigma}; \Delta\delta^{cr} = \Delta\lambda b. \frac{\delta G}{\delta\sigma} \tag{4}$$

The plastic multiplier increment $\Delta\lambda$ is determined by the consistency condition as

$$\Delta F=\frac{\delta F}{\delta\sigma} \cdot \left[k_e \cdot \left(\Delta\delta-\Delta\lambda\frac{\partial G}{\partial\sigma}\right)+\left(\frac{\partial k_e}{\partial\delta^p} \cdot \Delta\lambda\frac{\partial G}{\partial\sigma}\right) \cdot \delta^e\right]+\frac{\partial F}{\partial\xi} \cdot \frac{\partial\xi}{\partial\delta^p}.\Delta\lambda\frac{\partial G}{\partial\sigma}=0 \tag{5}$$

where, $\xi=\left[\tan\phi \quad c \quad f_t\right]^T$ is the vector of the internal variables controlling the evolution of the yield surface. Hence $\Delta\lambda$ and the plastic displacement increment can be expressed as

$$\Delta\lambda = \frac{(\partial F/\partial\sigma)\cdot k_e\cdot\Delta\delta}{H' + (\partial F/\partial\sigma)\cdot k_e\cdot(\partial G/\partial\sigma)} \tag{6}$$

$$\Delta\partial^p = \left(\frac{(\partial F/\partial\sigma)\cdot k_e\cdot\Delta\delta}{H' + (\partial F/\partial\sigma)\cdot k_e\cdot(\partial G/\partial\sigma)}\right)\frac{\partial G}{\partial\sigma} \tag{7}$$

in which H' is the effective plastic modulus given by

$$H' = -\frac{\partial F}{\partial\xi}\cdot\frac{\partial\xi}{\partial d^p}\cdot\frac{\partial G}{\partial\sigma} - \frac{\partial F}{\partial\sigma}\cdot\left(\frac{\partial k_e}{\partial\delta^p}\cdot\frac{\partial G}{\partial\sigma}\right)\cdot\delta^e \tag{8}$$

The first term is the classic plastic modulus due to the hardening/softening of the yield surface and the second term is due to the degradation of the effective elastic stiffness k_e. $H'<0$ for softening materials, $H'>0$ for hardening materials, $H'=0$ for perfect yielding materials. Substituting Eq. (6) and Eq. (7) into Eq. (3), the relationship between the traction increment and total separation increment can be obtained:

$$\Delta\sigma_i = \left[k_e - \frac{\left(k_e\cdot\frac{\partial G}{\partial\sigma}\right)\otimes\left(\frac{\partial F}{\partial\sigma}\cdot k_e\right)}{H' + \frac{\partial F}{\partial\sigma}\cdot k_e\cdot\frac{\partial G}{\partial\sigma}} + \frac{\left(\delta^e\cdot\frac{\partial k_e}{\partial d^p}\cdot\frac{\partial G}{\partial\sigma}\right)\otimes\left(\frac{\partial F}{\partial\sigma}\cdot k_e\right)}{H' + \frac{\partial F}{\partial\sigma}\cdot k_e\cdot\frac{\partial G}{\partial\sigma}}\right]\cdot\Delta\delta = k_{ep}\cdot\Delta\delta \tag{9}$$

where, $k_{ep}=k_e+k_p+k_d$ is the elastoplastic tangential stiffness matrix which is the linear combination of the effective elastic stiffness k_e, the plastic stiffness matrix k_p, and the coupled damage-plastic stiffness matrix k_d defined as:

$$k_e = \begin{bmatrix} k_n\left(1-d_n H(\sigma_n)\right) & 0 & 0 \\ 0 & k_{t1}\left(1-d_s H(\sigma_n)\right) & 0 \\ 0 & 0 & k_{t2}\left(1-d_s H(\sigma_n)\right) \end{bmatrix} \tag{10}$$

$$k_p = -\frac{\left(k_e\cdot\frac{\partial G}{\partial\sigma}\right)\otimes\left(\frac{\partial F}{\partial\sigma}\cdot k_e\right)}{H' + \frac{\partial F}{\partial\sigma}\cdot k_e\cdot\frac{\partial G}{\partial\sigma}} \tag{11}$$

$$k_d = \frac{\left(\delta^e\cdot\frac{\partial k_e}{\partial d^p}\cdot\frac{\partial G}{\partial\sigma}\right)\otimes\left(\frac{\partial F}{\partial\sigma}\cdot k_e\right)}{H' + \frac{\partial F}{\partial\sigma}\cdot k_e\cdot\frac{\partial G}{\partial\sigma}} \tag{12}$$

The coupled damage-plasticity traction separation law was implemented in ABAQUS [12] using user-subroutine VUINTERACTION for general contact interaction of the mortar joint interfaces.

3.3 Computational scheme

Due to the highly nonlinear nature of the simulation problem which includes nonlinear material responses, complicated and evolving constraints, contact among the components and geometric effects, the incremental dynamic analysis employs double-precision number and time increment of 0.01 secs to obtain sufficient accuracy. The prototype masonry structure was first excited at an intensity level of 0.1g and the subsequently increased at a rate of 0.1g and then the nonlinear analysis is continued till the maximum displacement is same with the increase in intensity level. A typical time history analysis of earthquake reveals that a number of steps are generated for a complete-time history analysis with a typical duration of 30-50 secs [16]. A large

number of data generated is impractical so save in the output file so the responses are saved at a certain time frame. Thus, the amount of data generated can be effectively reduced which is easier to manage without significant loss structural information for post-analysis.

For structures, System Identification (SI) can be invariably applied to identify structural parameters such as frequency, mode shape, damping ratio, stress and strain energy and structural response. In subspace system identification, extended observability matrix is determined from the Hankel matrices and the state-space model is estimated from the obtained extended observability matrix using LQ decomposition and singular value decomposition (SVD) [17]. Natural frequencies of the system are obtained from eigenvalues by eigenvalue decomposition of the system matrix. In this study, Recursive Stochastic Subspace System Identification (R4SID) is used because this technique takes less computational time by updating LQ decomposition and also a fixed-length of time can be used to capture the features of data for each step by step and the previous step results are used in the next step.

4. Performance of Structure under Considered Ground Motion

The nonlinear response histories for the masonry structure are analyzed in the context of five realistic ground motions. The earthquake records considered for this study are represented in Table 1 which represents a bin of relatively large magnitude of 6.5-7.6 and moderate distances effectively representing an earthquake scenario. The ground acceleration time history and elastic response spectrum (damping ratio=0.05) for all the five ground motions are represented in Fig. 3. In this bi-directional nonlinear time history analysis, the Z-direction of the structure is subjected to the stronger horizontal component of the ground motion, while the X-direction is subjected to the relatively weaker component. The natural frequency at the first mode of vibration determined by SI for unconfined and confined masonry structure is 14.71 Hz and 15.80 Hz respectively. Hence the corresponding time period (T_1) for unconfined and confined masonry structure was calculated as 0.068 secs and 0.063 secs respectively.

Table 1 – Details of the ground motion records considered (Source: PEER ground motion database https://ngawest2.berkeley.edu/) and corresponding spectral acceleration

Sl No	Event	Station	GM Label	Component	Rjb[1] (Km)	Vs30[2] (m/sec)	M[3]	Original PGA (g)	PGAh (g)	S_a/PGAh	
										$T_1=T_1$ CM	$T_1=T_1$ UCM
1.	Imperial Valley, 1979	El Centro Array #13	EC#13	140	21.98	249.92	6.53	0.1172	0.1414	1.104	1.231
				230				0.1384		1.395	1.633
2.	Loma Prieta, 1989	Hollister Diff. Array	HL	165	24.52	215.54	6.93	0.2687	0.2949	0.846	0.838
				255				0.2785		0.927	0.964
3.	Loma Prieta, 1989	Sunnyvale Cotton Ave	SV	270	23.92	267.71	6.93	0.2070	0.2191	1.065	1.028
				360				0.2071		0.998	0.985
4.	Kobe, 1995	Fukushima	FK	000	17.85	256	6.9	0.1821	0.2252	0.113	0.114
				090				0.2137		0.176	0.175
5.	Chi-Chi, 1999	CHY028	CH028	E	3.12	542.61	7.62	0.6282	0.7584	1.145	1.013
				N				0.7571		1.192	1.128

[1]Closest distance to the horizontal projection of the earthquake rupture plane (Joyner-Boore distance)
[2]Time averaged shear wave velocity in top 30m of the geomaterial
[3]Moment Magnitude

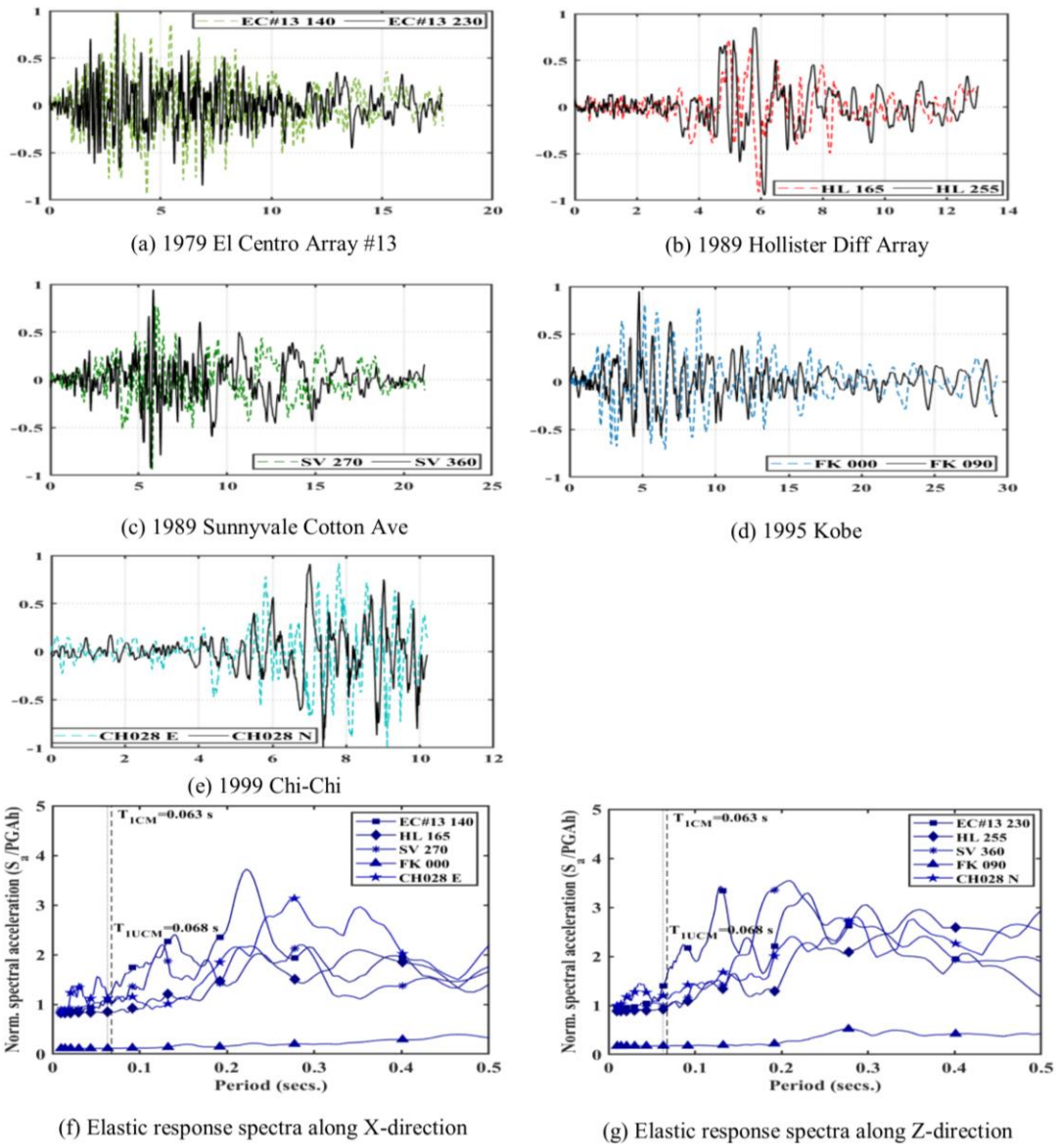

(a) 1979 El Centro Array #13

(b) 1989 Hollister Diff Array

(c) 1989 Sunnyvale Cotton Ave

(d) 1995 Kobe

(e) 1999 Chi-Chi

(f) Elastic response spectra along X-direction

(g) Elastic response spectra along Z-direction

Fig. 3 – Characteristics of ground motion considered for Incremental Dynamic Analysis [in the time history plot: vertical axis is ground acceleration (g) and horizontal axis is time (secs)].

4.1 Incremental dynamic analysis

The concept of incremental dynamic analysis is to monotonically scale up the considered ground motion until the response of the structure shows collapse. The monotonic scalable ground motion intensity measure (IM) is plotted against damage measure (DM) to derive an incremental dynamic analysis (IDA) curve. In this study, the IM considered is spectral acceleration [$S_a(T_1,5\%)$] at first mode period (damping considered as 5%) and the DM is the maximum drift ratio of the structure. Fig. (4) -Fig. (5) shows the IDA curves with severe damage point for confined and unconfined masonry structure along X and Z direction respectively. Comparing the IDA curves, it is observed that the roof drift is drastically reduced for confined masonry structure. This is due to the ductility and lateral in-plane load resistance provided by the tie columns which significantly improves the performance of masonry structure. Table 2 represents spectral acceleration at first-mode vibration and corresponding PGA for confined and unconfined masonry structure corresponding to severe damage state (SDS).

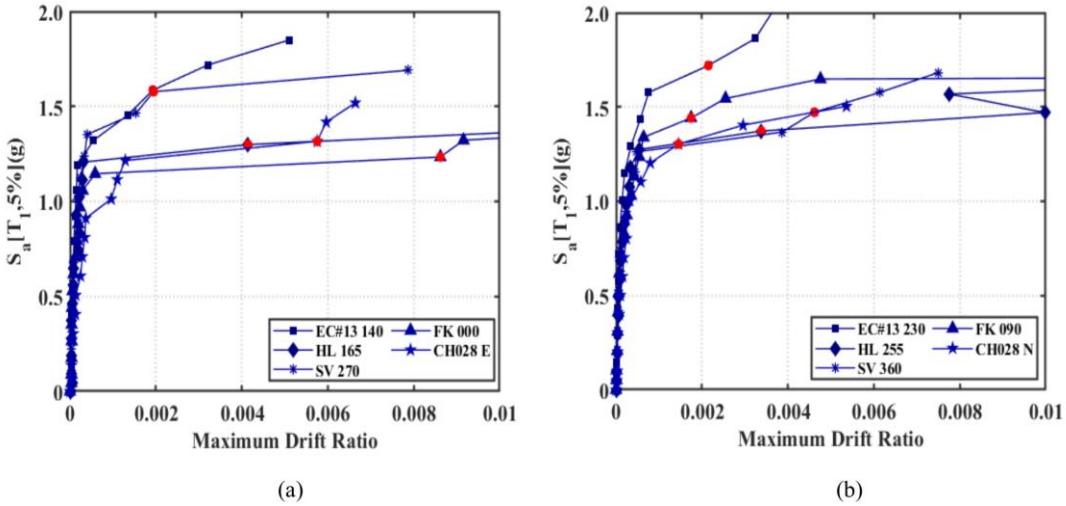

Fig. 4 – IDA curves of confined masonry structure for the considered ground motion along (a) X-direction and (b) Z-direction [(•) represents the 'severe damage'].

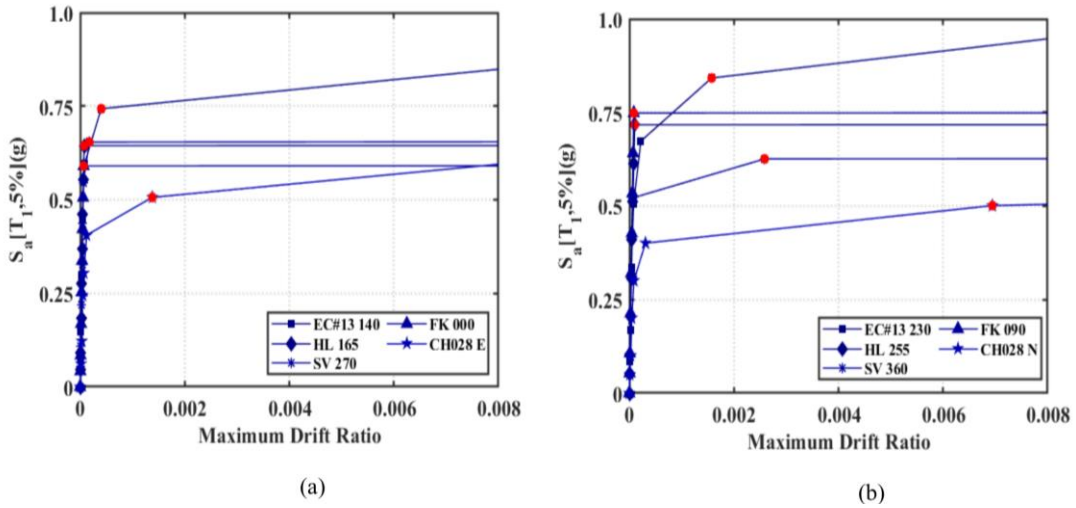

Fig. 5 – IDA curves of unconfined masonry structure for the considered ground motion along (a) X-direction and (b) Z-direction [(•) represents the 'severe damage'].

4.2 Effect of wall opening on stress distribution and damage pattern

The failure modes and minimum principal stress for confined and unconfined masonry structures are represented in Fig. (6) and Fig. (7). The simulation can effectively capture diagonal cracking of the masonry wall and failure near openings. Higher stress concentration around the openings causes ratcheting phenomena which cause sliding cracks. Walls with door opening have weaker initial bracing action compared to windows but after the masonry wall suffers severe damage due to the development of major cracks or partial collapse, the door opening becomes much stronger than the window. Thus, the structural damage of walls with door openings is less than that incurred on the walls with window opening due to reduced disintegration of wall components. In unconfined masonry structure, the masonry wall topples at a higher intensity level generally through poor roof-wall connection and propagates through weaker mortar joint which results in the collapse of the structure. The unrestrained sliding of masonry walls causes large variation in load transfer mechanism resulting in the larger displacement of the structure under bi-directional lateral loading.

Table 2 – Maximum attainable spectral and ground accelerations at SDS

Sl No.	Ground motion	Confined masonry structure				Unconfined masonry structure			
		X-direction		Z-direction		X-direction		Z-direction	
		S_a (g)	PGA (g)	S_a (g)	PGA (g)	S_a (g)	PGA (g)	S_a (g)	PGA (g)
1.	EC#13	1.586	1.2	1.720	1.2	0.743	0.5	0.842	0.5
2.	HL	1.300	1.4	1.372	1.4	0.644	0.7	0.717	0.7
3.	SV	1.578	1.4	1.472	1.4	0.654	0.6	0.626	0.6
4.	FK	1.234	1.4	1.442	1.4	0.590	0.7	0.748	0.7
5.	CH028	1.316	1.3	1.303	1.3	0.506	0.5	0.501	0.5

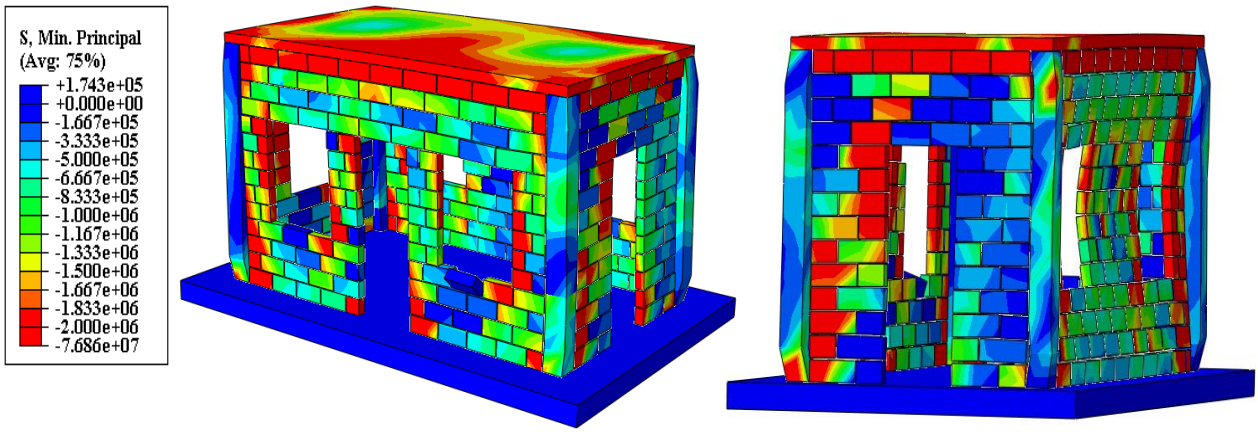

(a)

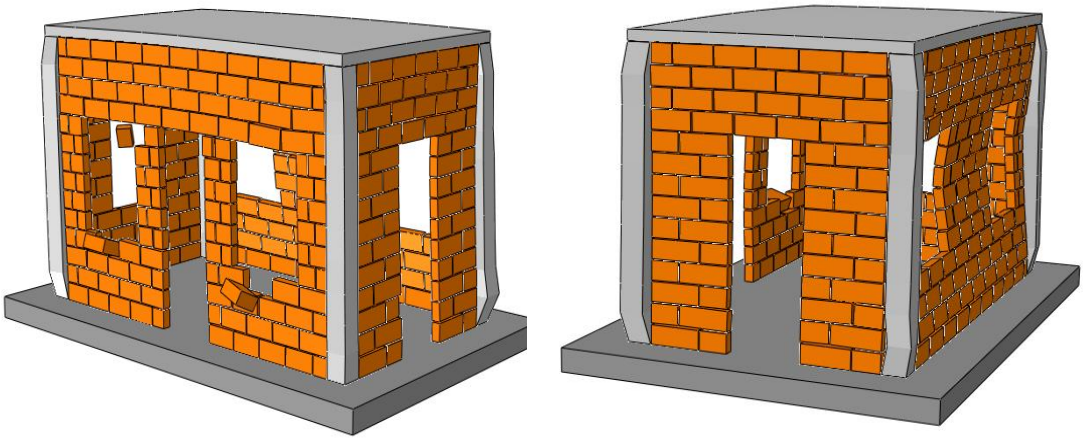

(b)

Fig. 6 – Evolution of simulated structural response and damage pattern for confined masonry structure at step time = 8.0 s (total time = 16.0 s) under bi-directional FK ground motion at $S_a[T_1,5\%] = 1.8g$ (deformation exaggerated 2 times): (a) minimum principal stress (N/m^2) (b) damage pattern of masonry wall and reinforced concrete columns.

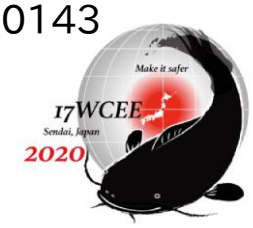

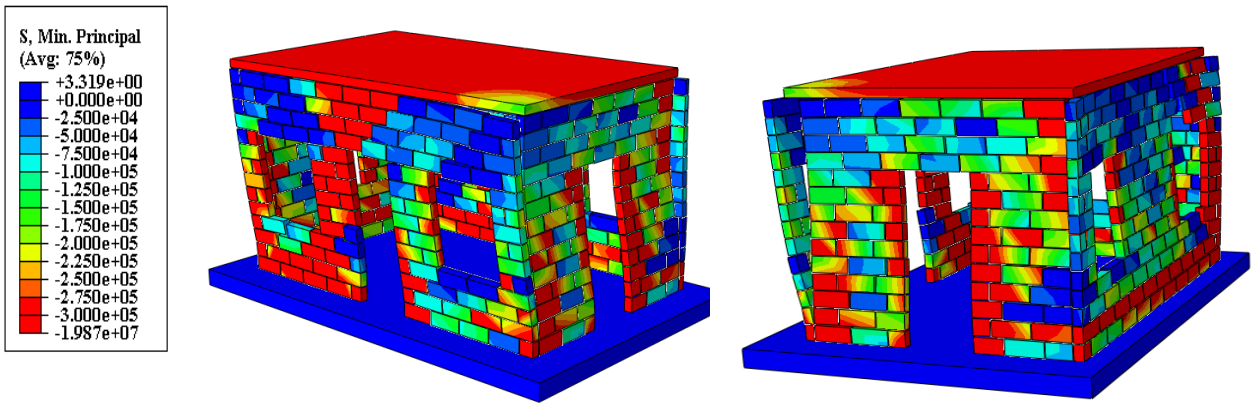

(a)

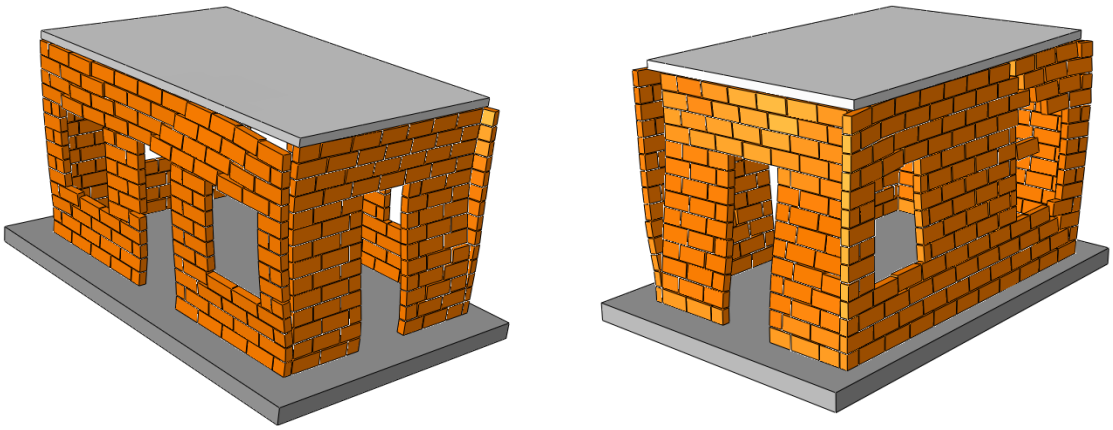

(b)

Fig. 7 – Evolution of simulated structural response and damage pattern for unconfined masonry structure at step time = 4.2 s (total time = 16.0 s) under bi-directional FK ground motion at $S_a[T_1,5\%] = 1.6g$ (deformation exaggerated 2 times): (a) minimum principal stress (N/m^2) (b) damage pattern of masonry wall.

5. Conclusion

The objective of this study is to assess the seismic performance and collapse probability of masonry structures under the influence of seismic excitation. Incremental dynamic analysis was performed with five different ground motions for the prototype masonry structures implemented in ABAQUS [12] using subroutine VUINTERACTION. Based on analysis results and discussions, the following conclusion can be drawn:

a) The curvature of the IDA curves shows that the collapse of confined masonry structure occurs gradually whereas the unconfined structure fails suddenly without early signs thereby posing vulnerability to the structure.

b) Masonry wall with door and window opening undergo cracks or ratcheting phenomena due to the propagation of sliding cracks initiated due to stress concentration around the corner of the openings. This phenomenon and consequent failure can be ceased for window openings due to kinematic restraint imposed by continuous wall beneath the opening.

c) Out-of-plane resistance of masonry structure can be enhanced by providing horizontal dowels or RC tie-beams. This results in a better load transfer mechanism and increases lateral stability of structure thereby ensuring progressive disintegration of the structure and increased collapse time.

d) The performance of confined masonry structure can be improved by providing better bonding between the masonry walls and adjacent RC columns.

6. Acknowledgment

The support of the Ministry of Science and Technology (MOST), R.O.C. under Grand Numbers 107-2636-E-009-002- and 108-2636-E-009-005- are gratefully acknowledged.

7. References

[1] Rahman A, Ueda T. (2014): Experimental Investigation and Numerical Modeling of Peak Shear Stress of Brick Masonry Mortar Joint under Compression. *Journal of Materials in Civil Engineering,* **26**(9), 04014061-1-13.

[2] Meli R, Brzev S, Astroza M, Boen T, Crisafulli F, Dai J, *et al.* (2011): *Seismic Design Guide for Low-Rise Confined Masonry Buildings*. Earthquake Engineering Research Institute (EERI), Oakland, California.

[3] Marques R, Lourenço PB. (2014): Unreinforced and confined masonry buildings in seismic regions: Validation of macro-element models and cost analysis. *Engineering Structures*, **64**, 52–67.

[4] Tomaževič M, Klemenc I. (1997): Seismic behaviour of confined masonry walls. *Earthquake engineering and Structural Dynamics,* **26**, 1059–71.

[5] Alcocer SM, Arias JG, Vázquez A. (2004): Response assessment of mexican confined masonry structures through shaking table tests, *13th World Conference on Earthquake Engineering*, Vancouver BC., Canada .

[6] Ghaisas K V., Basu D, Brzev S, Pérez Gavilán JJ. (2014): Strut-and-Tie Model for seismic design of confined masonry buildings. *Construction and Building Materials*, **147**, 677–700.

[7] Lourenço PB, Rots JG, Blaauwendraad J. (1998): Continuum model for masonry: Parameter estimation and validation, *Journal of Structural Engineering*, **124**, 642–652.

[8] Yuen YP, Kuang JS (2013). Fourier-based incremental homogenisation of coupled unilateral damage-plasticity model for masonry structures. *International Journal of Solids and Structures*, **50** (20–21), 3361-3374.

[9] Andreotti G, Graziotti F, Magenes G. (2018): Detailed micro-modelling of the direct shear tests of brick masonry specimens: The role of dilatancy. *Engineering Structures*, **168**, 929–949.

[10] D'Altri AM, de Miranda S, Castellazzi G, Sarhosis V. (2018): A 3D detailed micro-model for the in-plane and out-of-plane numerical analysis of masonry panels. *Computers and Structures*, **206**, 18–30.

[11] Yuen TYP, Deb T, Zhang H, Liu Y. (2019): A fracture energy based damage-plasticity interfacial constitutive law for discrete finite element modelling of masonry structures. *Computers and Structures*, **220**, 92–113.

[12] ABAQUS Inc. (2014): Abaqus User Subroutines Reference Guide.

[13] Sirca GF, Adeli H. (2012): System identification in structural engineering. *Scientia Iranica*, **19**(6), 1355–1364.

[14] CEB-FIP. *Model Code* (2010): Final version, Bulletin 66, Volume I, Lausanne, Switzerland.

[15] Rahman A, Ueda T, Walstra P, Wouters JTM, Geurts TJ, Gabor A, *et al*. (2017): Simulating masonry wall behaviour using a simplified micro-model approach. *Engineering Structures*, **151**, 349-365.

[16] Yuen YP, Kuang JS. (2015): Nonlinear seismic responses and lateral force transfer mechanisms of RC frames with different infill configurations. *Engineering Structures*, **91**, 125–140.

[17] Sloan SW, Abbo AJ, Sheng D. (2001): Refined explicit integration of elastoplastic models with automatic error control. *Engineering Computations,* **18**, 121–194.

[18] Loh CH, Weng JH, Liu YC, Lin PY, Huang SK. (2011): Structural damage diagnosis based on on-line recursive stochastic subspace identification. *Smart Materials and Structures*, **20**, 1-10.

